Theor Chem Acc (2015) 134:6
DOI 10.1007/s00214-014-1607-1

REGULAR ARTICLE

QCT dynamics study of the reaction of hydroxyl radical and methane using a new ab initio fitted full-dimensional analytical potential energy surface

Joaquin Espinosa-Garcia · Jose C. Corchado

Received: 25 September 2014 / Accepted: 11 December 2014 / Published online: 13 January 2015

Abstract In the present work, we have developed a new analytical potential energy surface fitted to ab initio data for the seven atoms OH + CH_4 → H_2O + CH_3 hydrogen abstraction reaction and its isotopomer analogues, named PES-2014. This surface provides analytically not only energy, but gradients, which is a computational advantage in dynamics calculations. It reproduces the topology of the reaction from reactants to products, with a barrier height of 6.4 kcal mol^{-1}, exothermicity of −13.3 kcal mol^{-1}, and the presence of intermediate complexes in the entrance and exit channels, in excellent agreement with recent accurate estimates and ab initio calculations. Using the PES-2014 surface, we performed quasi-classical trajectory calculations, in the collision energy range 4.0–16.0 kcal mol^{-1}, to analyze the dynamics of this reaction and its isotopomer analogue, OH + CD_4 → HOD + CD_3, comparing the results with experimental data. We analyze the excitation function, the product energy distribution, and the product angular distribution, obtaining reasonable agreement with the experimental information. Although the agreement is not yet quantitative, we conclude that the new PES-2014 surface and the QCT approach simulate reasonably well the dynamics of this reaction. Finally, by analyzing the role of the intermediate complexes in the dynamics, we find that the influence of the reactant complex is negligible while the product well permits randomization of the scattering angles for a small percentage (5–10 %) of the reactive trajectories that show a practically isotropic behavior, associated with an indirect mechanism.

J. Espinosa-Garcia (✉) · J. C. Corchado
Departamento de Quimica Fisica, Universidad de Extremadura, 06071 Badajoz, Spain
e-mail: joaquin@unex.es

Keywords Potential energy surface · Quasi-classical trajectory calculations · Reaction mechanisms · Comparison with experiment

1 Introduction

Full-dimensional quantum mechanical (QM) scattering description of triatomic systems of the type A + BC → AB + C is a relatively mature field, with results comparable to very precise experiments, and in recent years, promising QM advances have been carried out for tetra-atomic systems, AB + CD → ABC + D. The F + H_2 and the OH + H_2 reactions, and their isotopic variants, have served as benchmarks for such processes. However, the extension to full-dimensional polyatomic systems ($N > 4$) is today a very difficult (or prohibitive) problem, where the alternatives are reduced-dimensionality QM or quasi-classical trajectory (QCT) calculations.

Related to the dynamics (QM or QCT) method is the development of the full-dimensional potential energy surface (PES) describing nuclear motion, where the quality of the dynamics results strongly depends on the accuracy of the PES. Although Nyman and Clary [1] had previously developed a reduced-dimensional PES where the CH_3 group was treated as a pseudoatom, the first full-dimensional analytical PES for the OH + CH_4 → H_2O + CH_3 hydrogen abstraction reaction was developed by our group in 2000 and was named PES-2000 [2].

Additionally, PES-2000 has been used as a testing bench for different kinetics and dynamics studies: quantum instanton [3] and ring polymer molecular dynamics [4] calculations of rate constants; and dynamics reduced-dimensionality QM calculations of 5D [5], 6D [6], and 7D [7]. Additionally, PES-2000 has been tested against experimental kinetics and

dynamics studies. Srinivasan et al. [8] measured the rate constants of the title reaction using the reflected shock tube technique with multipass absorption spectrometric detection of OH radicals and found excellent theory/experiment agreement, within ±15 % of one another over the temperature range 250–2,000 K. That same year, Kopin Liu's laboratory [9–11] published a series of three papers which experimentally studied the dynamics of the OH + CD_4 reaction and its isotope effects at different collision energies and found that excitation of vibrational modes agrees with the theoretical predictions of PES-2000. In addition, they found HOD product backward scattering correlated with $CD_3(v = 0)$ coproduct, which shifts toward forward with the isotopic variant, OH + CH_4, and the collision energy.

However, despite the good kinetics and dynamics results obtained with this surface, it has a serious drawback, namely it is semiempirical, i.e., it was fitted using theoretical and experimental information, and it did not include information on the intermediate complex found on the reaction path. In the present paper, we construct a new PES for the seven atoms OH + CH_4 reaction and its isotopic variants based exclusively on ab initio calculations, to correct the main limitations of the previous PES-2000. First, we test the quality of the new surface, PES-2014, against the ab initio information used in the fit, and second, we perform QCT dynamics calculations and compare the results with the available experimental results from Kopin Liu's laboratory [9–11]. Finally, we analyze the role of the intermediate complexes in the entrance and exit channels on the reaction dynamics.

2 Full-dimensional potential energy surface

We constructed the new PES following the methodology developed by our group, which presents two different steps: functional form and fitting. The functional form is the sum of four terms:

$$V = V_{\text{stret}} + V_{\text{val}} + V_{\text{op}} + V_{\text{H}_2\text{O}} \tag{1}$$

This functional form was used in the previous PES-2000 surface, and the terms were developed there [2]. In brief, V_{stret} consists of four London–Eyring–Polanyi (LEP) stretching terms,

$$V_{\text{stretch}} = \sum_{i=1}^{4} V_3\left(R_{\text{CH}_i}, R_{\text{CO}}, R_{\text{H}_i\text{O}}\right) \tag{2}$$

which depend on 12 fitting parameters; V_{val} represents the harmonic bending terms,

$$V_{\text{harm}} = \frac{1}{2}\sum_{i=1}^{3}\sum_{j=i+1}^{4} k_{ij}^0 k_i k_j \left(\theta_{ij} - \theta_{ij}^0\right)^2 \tag{3}$$

Table 1 Saddle-point properties and reaction energy for the OH + CH_4 reaction

Method	R(C–H′)	R(O–H′)	$\Delta E^{\neq}$	ΔE_R	References
MP2-SAC	1.183	1.324	7.9	−13.3	[35]
MP2/TZ	1.181	1.330	6.1	−12.1	[36]
CBS/APNO	1.173	1.390	5.1	−13.5	[37]
G2M	1.233	1.286	5.3	−14.1	[38]
Database			6.7	−13.5	[14]
PES-2000	1.317	1.290	6.6	−13.3	[2]
CCSD(T)/TZ	1.184	1.315	5.8	−12.5	[15]
CCSD(T)-SAC	–	–	6.7	−13.5	[15]
CCSD(T)-EB	1.184	1.335	6.3	−12.4	[12]
W4	–	–	6.1–6.5	–	[13]
CCSD(T)-F12a	1.206	1.321	6.3[a]	−13.2[a]	[6]
IB	1.206	1.281	5.9	−13.1	This work
PES-2014	1.301	1.365	6.4	−13.3	This work

R(C–H′) and R(O–H′), in angstrom, represent the bond broken and formed in the reaction. ΔE_R, in kcal mol^{-1}, is the classical reaction energy. $\Delta E^{\neq}$, in kcal mol^{-1}, is the classical barrier height

[a] Hua Guo. Private communication

which depend on 16 fitting parameters; V_{op} is an a harmonic out-of-plane potential depending on four fitting parameters and given by

$$V_{\text{op}} = \sum_{i=1}^{4} f_{\Delta_i} \sum_{\substack{j=1 \\ j\neq i}}^{4} \left(\Delta_{ij}\right)^2 + \sum_{i=1}^{4} h_{\Delta_i} \sum_{\substack{j=1 \\ j\neq i}}^{4} \left(\Delta_{ij}\right)^4 \tag{4}$$

and finally, $V_{\text{H}_2\text{O}}$ is the potential describing the water product, which consists of two terms, a Morse potential describing the O–H bond in the hydroxyl radical and a harmonic potential describing the H–O–H bending, and depends on three new parameters. In addition, a series of switching functions are included to allow relaxing from methane to methyl radical and from hydroxyl radical to water. The functional form, Eq. 1, is symmetric with respect to the permutation of the four hydrogens in methane, and in addition to the energy of the system, it also provides analytical gradients, i.e., first energy derivatives, which is an advantage for dynamics calculations. Therefore, the new PES depends on 35 parameters, which give great flexibility to the PES while keeping the functional form physically intuitive.

The main difference between the new PES-2014 and the old PES-2000 lies in the fitting procedure of the 35 parameters. While the older surface was semiempirical in nature, i.e., it was fitted using theoretical and experimental data, the new PES-2014 is fitted exclusively to ab initio calculations. One of the most sensitive points in the topology of the reaction is the saddle-point description, and Table 1 lists some representative and recent results from the literature.

Firstly, the barrier height is strongly dependent on the level (correlation energy + basis set) used, with values in the range 5.0–7.9 kcal mol^{-1}, although the more recent and accurate ab initio results [6, 12, 13] give values in the narrower range 6.1–6.5 kcal mol^{-1}, in agreement with the best estimate from Truhlar's group [14], 6.7 kcal mol^{-1}. Secondly, these results highlight the difficulty in correctly describing the saddle point for this reaction, and even ab initio calculations at the CCSD(T)/aug-cc-pVTZ high level [15] slightly underestimate the barrier. Obviously, this problem increases when hundreds or thousands of ab initio calculations are necessary to describe the reactive system.

In the present work, we use a more economic alternative, dual-level calculations, where the geometry and vibrational frequency are calculated at the PMP2/6-31G(d,p) level, while the energy, computationally more expensive, is calculated at a high level using the "infinite basis" (IB) method [16, 17] for extrapolation to a complete one-electron basis set for correlated electronic structure calculations. This method is based on the extrapolation of energies obtained by using correlation-consistent polarized double- and triple-zeta basis sets [18], cc-pVDZ and cc-pVTZ. The extrapolated energies are more accurate and more economical computationally speaking than even larger basis sets [13, 16]. Despite its low computational cost, the barrier height, 5.9 kcal mol^{-1} (Table 1), reproduces more expensive results [15] and is only slightly lower than the more exact results [12, 13], 6.1–6.5 kcal mol^{-1}.

On the other hand, the presence of intermediate complexes in the entrance and exit channels may have an influence on the dynamics description, and they were not considered in the fitting of the previous PES-2000 surface. With the IB method, the reactant complex (RC) presents a stabilization of −0.45 kcal mol^{-1} with respect to the reactants and an H_3C–H…OH configuration. Another reactant complex has been previously reported [15, 19, 20], but with a different configuration, H_4C…HO, which is not on the minimum energy path for the hydrogen abstraction reaction. The product complex (PC) is stabilized by 1.8 kcal mol^{-1} with respect to the products and presents an H_3C…HOH configuration. This complex was previously reported by Masgrau et al. [15] stabilized by around 2 kcal mol^{-1}.

Finally, we analyze classical reaction energy, which presents a narrower range of values than barrier height, i.e., it is less dependent on level of calculation. In the literature, we find values (Table 1) ranging between −12.1 and −14.1 kcal mol^{-1}, with the IB method giving −13.1 kcal mol^{-1}, which reproduces recent accurate ab initio results [6], −13.2 kcal mol^{-1}, and the best estimate from Truhlar's group [14], −13.5 kcal mol^{-1}. In sum, the IB method gives an energetic description within the range of benchmark values in sensible points of the PES, which gives confidence to its results. However, as these values will be used in the fitting procedure of the PES, it is necessary to take into account that the usability of this surface depends not only on the accuracy of the energies, but also on the capability of the analytical function to reproduce these values used for the fitting procedure. Because of the uncertainties introduced by the fitting and the functional form, other factors, such as the spin contamination, the basis set superposition error (especially important in the description of the intermediate complexes), or the multiconfigurational character of the wavefunction, are not taken into account. Nevertheless, in view of our previous experience and the results obtained in the present paper, we suppose that their influence is small, and including these factors is not worth the additional computational cost.

Therefore, with the IB method, we optimize and characterize all stationary points (reactants, reactant complex, saddle point, product complex, and products) and additionally we calculate the minimum energy path (MEP). To describe the reaction valley, we also compute the gradients and Hessians for 60 points along the MEP. This method calculates the first and second energy derivatives analytically, which would be equivalent in a numerical calculation to 441 calculations of energy per point (441 is 21 squared, and 21 is 3 coordinates per atom times 7 atoms). As we calculate 60 points, this represents about 25,000 energy calculations, considering also the description of all stationary points. All the ab initio information previously described was used in the fitting procedure.

3 Results and discussion

3.1 Accuracy of the fitting

Firstly, we test the quality of the PES-2014 against the ab initio information used in the fitting, which is a test of consistency. Figure 1 plots a schematic diagram of the reaction path, from reactant to products, and Fig. 2 shows the structure of the saddle point and the intermediate complexes. PES-2014 reproduces reasonably the ab initio structures of these stationary points, with the largest difference at the C–H′–O bending angle of the saddle point. The breaking C–H′ bond is shorter than the forming O–H′ bond reproducing the ab initio information, and therefore, it improves the PES-2000 description, which gives the opposite behavior. Energetically, PES-2014 reproduces the IB values of all stationary points, and the barrier height is closer to the benchmark values [6, 12–14]. Agreement in reaction energy is very good, −13.3 versus −13.5 kcal mol^{-1}, and when we consider reaction enthalpy at 0 K, we obtain −14.9 kcal mol^{-1}, thus reproducing the experimental evidence [21], −14.7 kcal mol^{-1}. This comparison with ab

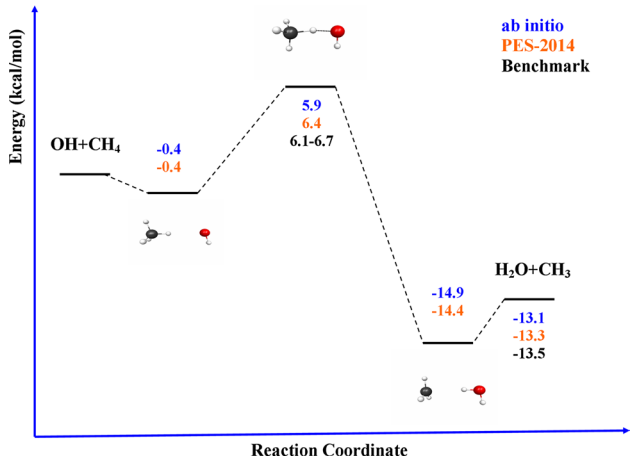

Fig. 1 Schematic profile of the potential energy surface for the OH + CH_4 → H_2O + CH_3 reaction. Benchmark values from Ref. [13, 14]

initio information indicates that the PES functional form and fitting procedure describe reasonably well the reactive system.

Figure 3 plots the energy variation along the MEP for PES-2014 and the IB method. The MEP obtained with the PES-2000 surface is also included for comparison. The topology of the reaction reproduces the ab initio calculations using the IB method, and the fall in the exit channel improves with respect to the PES-2000, which is very repulsive. This behavior has no consequences with regard to the kinetics results, which depend mainly on the transition state zone, but it does have consequences on the dynamics, because this fall permits a larger vibrational energy to be available to the products. Note that topology in the entry channel is well described by both analytical PESs. At present, the new PES-2014 surface can be obtained upon request to the authors.

3.2 Dynamics calculations

3.2.1 Computational details

Firstly, because more experimental information is available, we performed QCT calculations, using the VENUS-96 code [22, 23] and the new PES-2014, for the OH + CD_4 → HOD + CD_3 reaction at collision energies in the range 4.0–16.0 kcal mol^{-1} (seven energies) for a direct comparison with Liu's group experiments [9–11]. At each collision energy, we ran 100,000 trajectories with an initial separation between the reactants of 10.0 Å, the trajectory finishing when the C–O distance was 12.0 Å. At each collision energy, the maximum impact parameter, bmax, was obtained systematically by increasing the value of b until no reactive trajectories were found. The values of

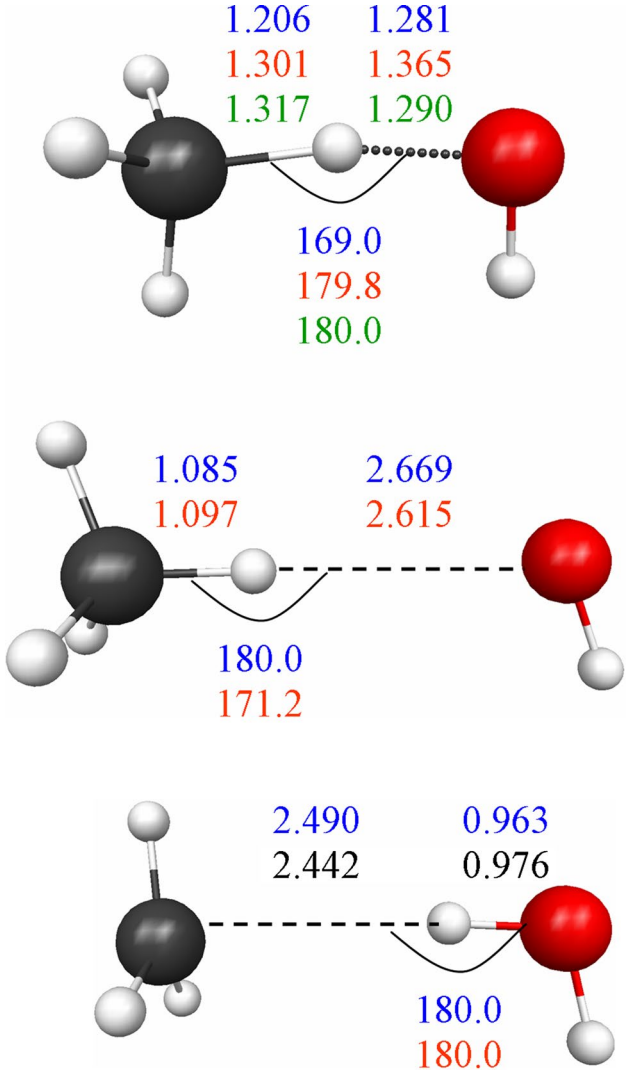

Fig. 2 Geometries of the saddle point (*upper*), reactant complex (*middle*) and product complex (*lower*) for the OH + CH_4 reaction. The first entry, in *blue*, corresponds to the IB method [MP2/6-31G(d,p) level], the second entry, in *red*, corresponds to the PES-2014 surface, and the third entry, in *green*, corresponds to the PES-2000 surface. Distance in angstrom and angles in degrees

bmax vary from 2.2 to 2.5 Å. For the CD_4 reactant, vibrational energy was fixed at its zero-point energy value, i.e., 20.7 kcal mol^{-1}, while rotational energy was chosen by thermal sampling at 298 K. For the OH reactant, the rotational and vibrational quantum numbers were fixed at a value of 0, the ground state. Other scattering parameters, such as spatial orientation of the initial reactants, vibrational phases, and impact parameter, were selected via a Monte Carlo approach as implemented in VENUS-96, and the propagation time step was selected to ensure energy conservation, 0.2 fs.

Secondly, we completed the dynamics study by analyzing the isotope effects with the OH + CH_4 reaction. The

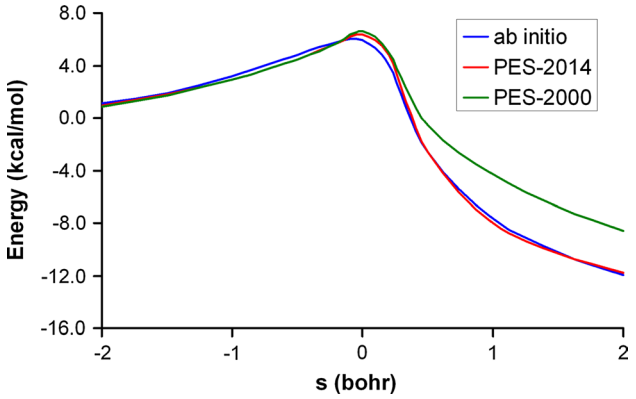

Fig. 3 Classical potential energy as a function of the reaction coordinate, s. *Blue line* ab initio results with the IB method; *red line* PES-2014 surface; and *green line* PES-2000 surface

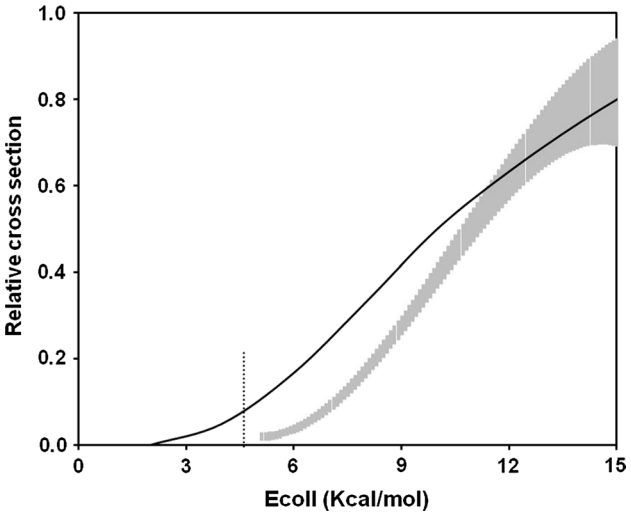

Fig. 4 Reaction cross section as a function of collision energy (kcal/mol). *Solid* and *dashed lines* represent QCT and experimental (Ref. 10) values, respectively, while the *vertical dashed line* at 4.6 kcal mol represents the activation energy at 298 K. For a direct comparison with the experiment, the QCT values are normalized at 16.0 kcal mol^{-1}, and the *shaded zone* represents experimental uncertainties

QCT initial conditions are similar, where CH_4 zero-point energy is 28.3 kcal mol^{-1}, and the bmax value is 2.8 Å at collision energy of 10.0 kcal mol^{-1}, the only experimental data reported [11]. We ran 100,000 new trajectories.

Thirdly, to analyze the effect of the OH reactant rotation on the dynamics, we performed QCT calculations at OH(j = 1,3,5), where 100,000 trajectories were run at each rotational quantum number.

Experimentally Kopin Liu's lab analyzed these reactive trajectories leading to the CD_3/CH_3 product in its vibrational ground state. For an accurate comparison, in the case of the $CD_3(v = 0)$ product, only reactive trajectories with vibrational energy below 14.9 kcal mol^{-1} (the energy needed to excite with one quantum the lowest vibrational mode of the CD_3 product is 396 cm^{-1}≈1.1 kcal mol^{-1}, which added to its ZPE, 13.8 kcal mol^{-1}, gives a total vibrational energy of 14.9 kcal mol^{-1}) were considered. In the case of the $CH_3(v = 0)$, the limit was 20.3 kcal mol^{-1} (CH_3 umbrella mode 510 cm^{-1}≈1.5 kcal mol^{-1} and ZPE 18.8 kcal mol^{-1}). Note that this strategy, which is not related to the popular histogram or Gaussian binning techniques, has already been used successfully in other reactions [24] and represents a good approximation as it ensures that these trajectories do not have sufficient energy to achieve even the first excited vibrational state of the CD_3/CH_3 product.

For both reactions, the reaction cross section is obtained by Eq. 5:

$$\sigma_R = \pi b_{\max}^2 \frac{N_r}{N_t} \tag{5}$$

where N_r and N_t are, respectively, the number of reactive and total trajectories. For the OH + CH_4 and OH + CD_4 reactions, we obtained values of 1.88 ± 0.02 and 0.91 ± 0.01 Å^2, respectively, at collision energy of 10.0 kcal mol^{-1}, and therefore a kinetic isotopic effect (KIE) of 2.06 ± 0.03. There are no experimental dynamics data for comparison at this energy, but the KIEs at different temperatures [25] present values higher than one, i.e., CH_4/CD_4 "normal" KIEs, related to the larger tunneling effect in the perprotio reaction.

Finally, the differential cross section (DCS) is given by

$$\frac{d\sigma_R}{d\Omega} = \frac{\sigma_R . P_r(\theta)}{2\pi \sin(\theta)} \tag{6}$$

where dΩ is an infinitesimal solid angle and $P_r(\theta)$ is the product normalized probability of trajectories with scattering angle θ. In the present work, the DCS is fitted by the Legendre moment method [26], which measures the angular scattering distribution of the HOD/H_2O products with respect to the incident OH reactant.

3.2.2 *Excitation function*

For the OH + CD_4 reaction, Fig. 4 plots the QCT excitation function, i.e., reaction cross section versus collision energy, in the energy range 4.0–16.0 kcal mol^{-1}, together with experimental data [10] for comparison. Note that since the experiment only reports relative cross sections, the QCT values are rescaled at the highest experimental value of 16.0 kcal mol^{-1}. First, in general, the QCT results reproduce the experimental shape, although at low collision energies the theoretical values present a softer fall. Second, the QCT results present reactivity below the activation energy, which is 4.6 kcal mol^{-1} at 298 K using the

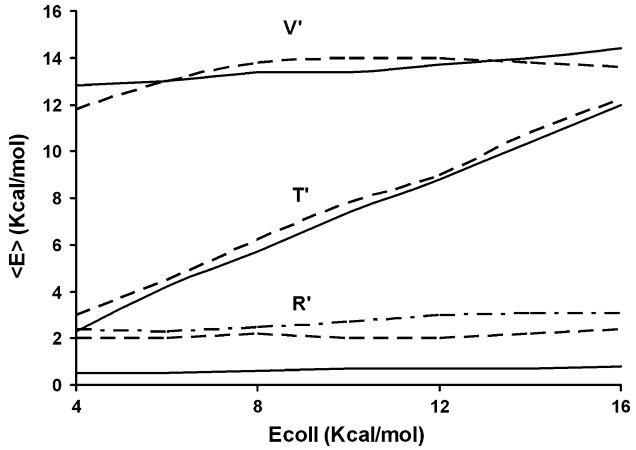

Fig. 5 Correlated HOD product energy disposal with collision energy for the $CD_3(v = 0)$ coproduct in the OH + CD_4 reaction. *Solid* and *dashed lines* represent the QCT and experimental [10] values, respectively. The *dashed-dotted line* in R' represents the average rotational energy deposited in the CD_3 coproduct, which was not reported in the experiment

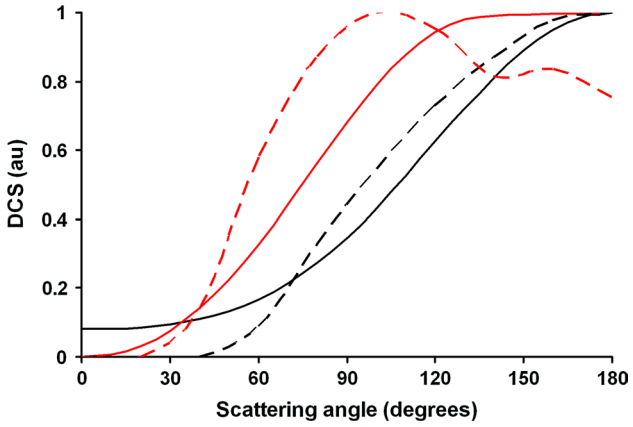

Fig. 6 HOD product angular distribution (with respect to incident OH) for the OH + CD_4 reaction. *Solid lines* QCT results from this work and *dashed lines* experimental data [9, 10]. *Black lines* QCT and experimental results at 10.0 kcal mol^{-1}; *red lines* QCT results at 16.0 kcal mol^{-1} and experimental values at 16.2 kcal mol^{-1}. For a direct comparison, all results are normalized to the highest value in each series

PES-2014 surface. Given the classical nature of the QCT calculations, this reactivity is artificial, because tunneling is not allowed in these calculations. We believe that the reason for the reactivity below the threshold is due to ZPE leakage [27], i.e., part of the vibrational energy is transferred to promote reactivity, leading to a system with a vibrational energy below its ZPE, which is not conserved because of the classical nature of the trajectory propagation methods. This artificial effect of the QCT calculations could explain the softer fall at low energies, which therefore seems to be related to the approximations of the QCT method rather than to deficiencies of the PES.

3.2.3 Correlated product energy partition

Figure 5 plots the QCT collisional energy dependency of the HOD product energy disposal correlated with the $CD_3(v = 0)$ coproduct in the OH + CD_4 reaction, together with the experiment [10] for comparison. While the average energy disposals in the vibrational (V′) and rotational (R′) HOD product are practically invariant with collision energy, translational (T′) energy increases with collision energy, showing a practically linear dependency. This behavior reproduces the experimental evidence [10], associated with the propensity T(or Ecoll) $\rightarrow T'$ of the heavy-light-heavy systems, which has a kinematic origin. The larger theory/experiment differences are found in the rotational energy. However, it is important to note that while in the experiment V' and T' are directly measured, R' is deduced by conservation of energy, assuming that CD_3 moiety is a structureless particle [10]. Our QCT results permit us to obtain the rotational energies for both the HOD and CD_3 products, which present uncertainties of ±10 and ±19 %, respectively. On the other hand, Liu et al. [28] observed that QCT results using VENUS code overestimate product rotational energy. Thus, taking into account these uncertainties, when the CD_3 rotational energy is added to R′ in Fig. 5, agreement with the experiment improves. Therefore, $CD_3(v = 0)$ coproduct rotational energy is not negligible in this reaction, and so the CD_3 moiety cannot be considered as a structureless particle, as previously supposed [10].

3.2.4 Product angular distribution

The HOD product scattering angle correlated with $CD_3(v = 0)$ coproduct in the OH + CD_4 reaction at two collision energies, 10.0 and 16.0 kcal mol^{-1}, is plotted in Fig. 6, together with the experiment reported by Kopin Liu's laboratory [9, 10] for comparison. At 10.0 kcal mol^{-1}, scattering presents a backward distribution, associated with low impact parameters and a rebound mechanism. In fact, the transition state is collinear, CD_3…D…OH, with a narrow cone of acceptance. When collision energy increases, the scattering angle shifts to the forward hemisphere, associated with a wider cone of acceptance, larger impact parameters and a stripping mechanism. This tendency reproduces the experimental evidence, although theoretically at high energy the shift to scattering forward is less pronounced, and the QCT results present a larger tail at lower scattering angles. Below (Sect. 3.2.6) we will further discuss this contribution in the forward region.

3.2.5 Isotope effects

Another dynamics property experimentally measured by Kopin Liu's laboratory [11] is the isotope effects. In this section, we compare the QCT results with the experiment for the OH + CH_4/CD_4 isotope effect at collision energy of 10.0 kcal mol^{-1}.

The H_2O/HOD product scattering angles correlated with CH_3/CD_3($v = 0$) coproduct are plotted in Fig. 7 at collision energy of 10.0 kcal mol^{-1} together with the experiment [11] for comparison. As was previously noted, the OH + CD_4 reaction presents backward scattering (Fig. 6), which shifts to the forward hemisphere with the isotope substitution, OH + CH_4. This tendency reproduces the experiment, although the shift is less pronounced than in the experiment. In the next section, we analyze the cause of the small contributions in the forward hemisphere in both reactions, OH + CH_4/CD_4, obtained with QCT calculations. Experimentally, Liu's laboratory [9–11] reported that scattering angles are confined mainly in the backward region with a small contribution in the forward hemisphere, due to the small reactive cross section in this region.

3.2.6 Role of the intermediate complexes in the dynamics

In Sect. 2 and Fig. 1, we showed the energetic profile of the hydrogen abstraction reaction, with the presence of intermediate complexes in the entrance and exit channels. What is the role of these complexes in the dynamics? Analysis of the individual reactive trajectories showed that two different mechanisms are possible in the OH + CH_4/CD_4 reaction: direct, with a brief encounter between the reactants and fast separation of the products; and indirect, where the reactive trajectories "visit" the wells. Both isotopes present similar behavior and therefore the results are analyzed together. In the indirect mechanism, we found that the influence of the reactant complex is negligible and all reactive trajectories "visit" only the product complex. Therefore, this product complex permits repeated encounters between the two products and after a certain time (which depends on the trajectory) the products separate. Figure 8 shows both mechanisms, where the evolution of the C–H′ (broken bond, dashed line) and H′–O (formed bond, solid line) distances as a function of time is represented. In the direct or impulse-type mechanism (upper panel), the OH collides with methane and forms the H_2O product which immediately recoils away. In the indirect mechanism (lower panel), the H_2O and methyl products undergo several collisions in the exit channel before leaving the well. Similar indirect mechanisms of reaction were found in our previous studies of the Cl(^{2}P) + NH_3 and OH + NH_3 reactions [29, 34], which also present wells in the entrance and exit channels. In these nearly trapped trajectories, the

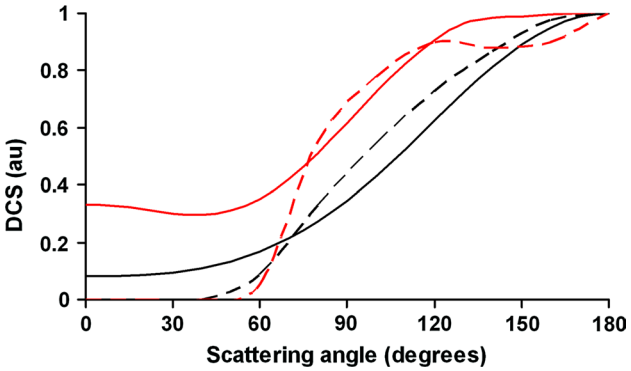

Fig. 7 H_2O/HOD product angular distribution with respect to incident OH reactant at collision energy of 10.0 kcal mol^{-1}. *Solid lines* QCT results from this work and *dashed lines* experimental data [11]. *Black lines* OH + CD_4 reaction and *red lines* OH + CH_4 reaction. For a direct comparison all results are normalized to the highest value in each series

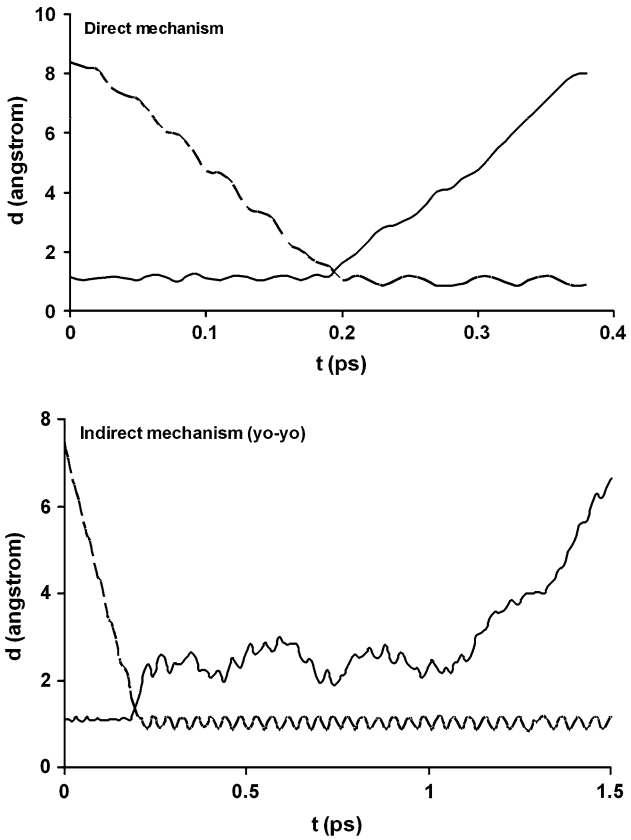

Fig. 8 Representative plots of direct (*upper panel*) and indirect (*lower panel*) mechanisms, shown as the evolution of the C–H′ (*dashed line*) and H′–O (*solid line*) distances as a function of time (ps)

products approach and move away repeatedly and after a certain time they separate definitively. These indirect trajectories are classically similar to the spring motion, they

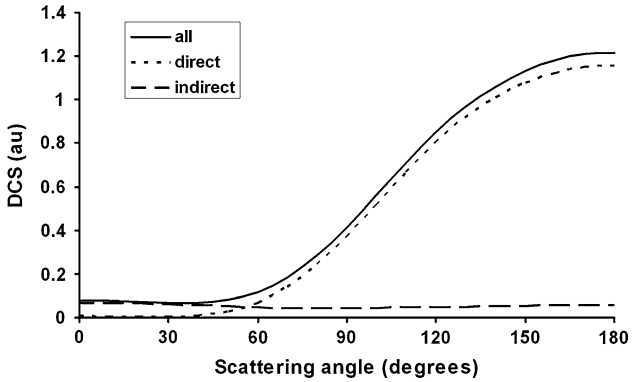

Fig. 9 HOD product angular distribution with respect to incident OH reactant at collision energy of 10.0 kcal mol^{-1} for the OH + CD_4 reaction. *Solid*, *dotted* and *dashed lines* correspond, respectively, to all trajectories, direct and indirect mechanism

Table 2 Reaction cross section (Å^2) for the OH + CH_4 reaction, at collision energy of 10 kcal mol^{-1}, as a function of the OH rotational number

OH(j)	σ_R	
	QCT[a]	QM[b]
0	1.88 ± 0.02	2.2
1	1.66 ± 0.02	1.8
3	1.11 ± 0.03	1.1
5	0.71 ± 0.03	0.7

[a] CT calculations from this work

[b] QM calculations from Ref. 6, read directly from Fig. 5a

are a straightforward consequence of the presence of wells, and we have named them the "yo–yo" mechanism, because of their resemblance to popular toy.

For visualization of individual trajectories, we quantify the importance of these mechanisms by using the average time of flight: ≤500 fs for direct and ≥500 fs for indirect. Obviously, these values are not absolute, but rather they serve as a simple reference to separate both mechanisms. Additionally, the indirect mechanism is related to multiple inner–outer turning points, which are absent in the direct mechanism. Using the collision energy of 10.0 kcal mol^{-1} for comparison with the experiments [9], we found that only about 5–10 % of the reactive trajectories follow the indirect mechanism, where the CH_4 reaction presents the highest percentages.

Product angular distribution is undoubtedly one of the most sensitive dynamics properties for analyzing the role of these mechanisms (and therefore the role of the intermediate complexes) in the reaction. For the OH + CD_4 reaction, the scattering distributions for direct (95 %) and indirect (5 %) mechanisms are plotted in Fig. 9 for the correlated $CD_3(v = 0)$ coproduct, together with the distribution for all trajectories. While the direct mechanism presents backward scattering, associated with a typical rebound mechanism, the indirect one shows a practically isotropic behavior. The perprotio variant, OH + CH_4, presents similar shapes, although the indirect trajectories have a slightly more forward tendency. This behavior indicates that the product well permits randomization of scattering angles, producing quasi-isotropic distributions, where the products "forget" the initial direction of approach. Considering the weights of both mechanisms, a backward distribution is mainly obtained when all reactive trajectories are analyzed.

Thus, the tail at low scattering angles obtained with QCT calculations (Sect. 3.2.5, Figs. 7, 9) is due to the indirect mechanism. This result confirms the experimental finding [9] in which the scattering distributions are confined mainly in the backward direction, with a small reactive cross section in the forward hemisphere.

3.2.7 *Effect of the reactant rotation on the dynamics*

Recently, Song et al. [6] performed reduced-dimensionality time-dependent wave packet calculations based on the PES-2000 surface [2] to analyze the effects of reactant rotation on the dynamics of the OH + CH_4 reaction. They found that while rotational excitation of methane has little effect, the rotational excitation of the OH inhibits reactivity. To the best of our knowledge, no experimental data are available for comparison.

To analyze the role of OH rotational excitation on reactivity, based on the PES-2014 surface, we performed QCT calculations at OH(j = 1,3,5) at collision energy of 10.0 kcal mol^{-1}, comparing the results with those previously obtained for OH(j = 0). The reaction cross sections for OH(j = 0,1,3,5) appear in Table 2, together with the QM results for comparison. We observe that reactivity decreases with the OH rotational excitation, thus reproducing the QM results reported by Song et al. [6]. The small differences are due to the approaches used in each case, QCT/QM and PES-2014/PES-2000.

Nobusada et al. [30], Schatz [31] and Zhang and Lee [32, 33] analyzed this effect in atom–diatom and diatom–diatom reactions. They concluded that in some reactions with linear saddle point, reactant rotational excitation disrupts the preferred linear approach, inhibiting reactivity, an effect known as "the orientation effect" [30]. In polyatomic reactions, such as OH + CH_4, the problem is more complicated due to dimensionality, but in this case the oxygen atom orientation is close to collinear with the H′–C bond in methane at the saddle point. Therefore, the decrease in reactivity with OH rotational excitation can be explained

by the "orientation effect." This effect has been confirmed by visualization of individual trajectories at OH($j = 0$) and OH(j = 1,3,5), where the larger rotational excitation in OH(j = 1,3,5) causes rotation of the OH reactant, and the multiple rotations disfavor the correct approach of the oxygen atom to the H′–C bond.

4 Conclusions

In this study, we performed ab initio calculations to describe all the stationary points for the title reaction, with special attention to description of the reactant and product complexes in the entrance and exit channels and of the saddle point. Additionally, we calculated the topology of the reaction, and we described the minimum energy path (energy) and the valley path (gradients and Hessians).

Using this ab initio information as input data, we developed a new full-dimensional analytical potential energy surface for the title reaction, PES-2014, which improves the older PES-2000 surface, which was semiempirical in nature, i.e., experimental and theoretical information was used in the fitting. The new PES-2014 reproduces the ab initio information used in the fitting process, which is merely a test of consistency, with a barrier height of 6.4 kcal mol^{-1}, in excellent agreement with recent and accurate estimates and ab initio calculations, 6.1–6.7 kcal mol^{-1}, with an exothermicity of −13.3 kcal mol^{-1}, reproducing accurate ab initio calculations, −13.1–(−13.5) kcal mol^{-1}, and, more importantly, the topology of the reaction, which has an influence on the vibrational distribution of the products. The PES-2014 provides energy and analytical gradients, which is an interesting and useful feature for speeding up dynamics calculations.

With the PES-2014, we performed a dynamics study using QCT calculations and compared the results with the experiment. We analyzed excitation function, product energy distribution and differential cross section for the OH + CD_4 reaction at different collision energies, and the isotope effect for the OH + CH_4 reaction at collision energy of 10.0 kcal mol^{-1}. In general, theory/experiment agreement is reasonable. Although this agreement is still qualitative, where discrepancies can arise from several sources, PES, QCT and approaches used, we believe that this potential energy surface represents an important step toward the understanding of polyatomic systems.

To complete this dynamics study, and as another test of the quality of PES-2014, a kinetics study is under development in our laboratory, in which rate constants and kinetic isotope effects will be analyzed by the variational transition state theory with multidimensional tunneling and the ring polymer molecular dynamics methods.

Finally, for visualization of the individual reactive trajectories, we observed in addition to the direct trajectories a small percentage (5–10 %) of indirect trajectories, with a larger time-of-fly, which "visit" the product well, and are responsible for the small contribution in the forward region experimentally observed.

References

1. Nyman G, Clary DC (1994) J Chem Phys 101:5756–5771
2. Espinosa-Garcia J, Corchado JC (2000) J Chem Phys 112:5731–5739
3. Wang W, Zhao Y (2012) J Chem Phys 137:214306
4. Allen JW, Green WH, Li Y, Guo H, Suleimanov Y (2013) J Chem Phys 138:221103
5. Yu H-G (2001) J Chem Phys 114:2967–2976
6. Song H, Li J, Jiang B, Yang M, Lu Y, Guo H (2014) J Chem Phys 140:084307
7. Song H, Lee S-Y, Yang M, Lu Y (2013) J Chem Phys 139:154310
8. Srinivasan NK, Su MC, Sutherland JW, Michael JV (2005) J Phys Chem A 109:1857–1863
9. Zhang B, Shiu W, Lin JJ, Liu K (2005) J Chem Phys 122:131102
10. Zhang B, Shiu W, Liu K (2005) J Phys Chem A 109:8983–8988
11. Zhang B, Shiu W, Liu K (2005) J Phys Chem A 109:8989–8993
12. Sellevag SR, Nyman G, Nielsen CJ (2006) J Phys Chem A 110:141–152
13. Karton A, Tarnopolsky A, Lamere J-F, Schatz GC, Martin JML (2008) J Phys Chem A 112:12868–12886
14. Lynch BJ, Fast PL, Harris M, Truhlar DG (2000) J Phys Chem A 104:4811–4815
15. Masgrau L, Gonzalez-Lafont A, Lluch JM (2001) J Chem Phys 114:2154–2164
16. Truhlar DG (1998) Chem Phys Lett 294:45–48
17. Fast PL, Sanchez ML, Truhlar DG (1999) J Chem Phys 111:2921–2926
18. Kendall RA, Dunning TH, Harrison RJ (1992) J Chem Phys 96:6796–6806
19. Basch H, Hoz S (1997) J Phys Chem A 101:4416–4431
20. Wheeler MD, Tsiouris M, Lester MI, Lendvay G (2000) J. Chem. Phys. 112:6590–6602
21. Chase MW, Davis CA, Downey JR, Frurip DJ, McDonald RA, Syverud AN (1985) JANAF Thermochemical tables, J Phys Chem Ref Data Suppl. 14(1):1–250
22. Hase WL, Duchovic RJ, Hu X, Komornicki A, Lim KF, Lu D-h, Peslherbe GH, Swamy KN, Vande Linde SR, Varandas AJC, Wang H, Wolf RJ (1996) VENUS96: a general chemical dynamics computer program. QCPE Bull 16:43
23. Hu X, Hase WL, Pirraglia Y (1991) J Comp Chem 12:1014–1024
24. Monge-Palcios M, Gonzalez-Lavado E, Espinosa-Garcia J (2014) J Chem Phys 141:094307
25. Gierczak T, Talukdar S, Herndon S, Vaghjiani GL, Ravishankara AR (1997) J Phys Chem 101:3125–3134
26. Truhlar DG, Blais NC (1977) J Chem Phys 67:1532–1539
27. Swamy KN, Hase WL (1983) J Phys Chem 87:4715–4720
28. Liu S, Chen J, Fu B, Zhang DH (2014) Theor Chem Acc 133:1–9
29. Monge-Palacios M, Yang M, Espinosa-Garcia J (2012) Phys Chem Chem Phys 14:4824–4834
30. Nobusada K, Moribayashi K, Nakamura H (1997) J Chem Soc Faraday Trans 93:721–726
31. Schatz GC (1981) J Chem Phys 74:1133–1139
32. Zhang DH, Lee S-Y (1998) J Chem Phys 109:2708–2716
33. Zhang DH, Lee S-Y (2000) J Chem Phys 112:203–211

34. Monge-Palacios M, Corchado JC, Espinosa-Garcia J (2013) J Chem Phys 138:214306
35. Truong TN, Truhlar DG (1990) J Chem Phys 93:1761–1769
36. Dobbs KD, Dixon DS, Komornicki A (1993) J Chem Phys 98:8852–8858
37. Malick DK, Peterson GA, Montgomery JA Jr (1998) J Chem Phys 108:5704–5713
38. Korchowiec J, Kawakara S, Matsumura K, Uchimaru T, Sugie M (1999) J Phys Chem A 103:3548–3553